J. Fluid Mech. (1973), *vol.* 60, *part* 4, *pp.* 641–664
Printed in Great Britain

An experimental investigation of a magnetically driven rotating liquid-metal flow

By T. ROBINSON
AB Atomenergi, Studsvik, Fack, Nyköping, Sweden

With an appendix by

KJELL LARSSON
AB Atomenergi, Studsvik, Fack, Nyköping, Sweden

(Received 26 March 1973)

Flow and turbulence in a 50 Hz rotating-field MHD system are investigated using the hot-film constant-temperature anemometer. Factors affecting anemometer disturbances and response time are discussed. From measurements of the magnetic field at points within the liquid the distribution of MHD forces is estimated. The mean rotational velocity of the flow is of the expected order of magnitude but much less dependent on the axial co-ordinate than the corresponding MHD force. With the aid of a thermal transit-time anemometer, a weak secondary flow is detected. A note on scale-model studies of MHD systems envisaged in metallurgical applications of magnetohydrodynamics points out some basic difficulties in modelling large high-powered systems on a small scale.

1. Introduction

Flow generated in a volume of liquid metal under the action of a rotating magnetic field has been treated theoretically by a number of authors, e.g. Moffatt (1965) and Dahlberg (1972), and is an essential feature of several recently envisaged applications of magnetohydrodynamics. The theoretical work has been limited to the case of laminar flow, but turbulent conditions are more usual in technical applications. These are mainly in metallurgy and include the intensification of mass transfer processes in metallurgical reactions, the improvement of the crystalline structure of castings, the centrifugation of sodium for gas or particle removal, etc. Examples of design and performance studies of equipment for such purposes may be found in reports by Vedkalov *et al.* (1971), Kapusta (1969), Rezin, Ermakov & Vetrov (1967), Gerlach (1972) and Hayes, Baum & Hobdell (1971).

Besides illustrating an extension of flow diagnostics, the present experimental study is aimed at providing turbulent-flow measurements which will be of interest not only to the hydrodynamicist but also to the engineer designing MHD-rotator equipment. An article by Briskman *et al.* (1970) on mean flow velocity in such systems summarizes previously available information obtained using Pitot tubes and manometers. In the present measurements a smooth-walled

closed cylinder of non-magnetic ($\mu/\mu_0 < 1{\cdot}03$) stainless steel was completely filled with mercury and placed coaxially within the stator of a three-phase induction motor. The mean azimuthal velocity and turbulence intensity were measured in the steady state at various points in the cylinder. Pitot-tube, hot-film, rotating-vane and thermal convection transit-time anemometers were employed, the latter in measurements of secondary flow velocities. The phases and amplitudes of the 50 Hz magnetic field components at various points within the mercury were measured with the aid of a small pick-up coil system, incorporating three coils with mutually perpendicular axes. From the field components the distribution of the MHD-force components within the volume was deduced. It was thus possible to study relations between the flow and the driving forces in the system. The power input to the system was limited so that the main, azimuthal mercury flow velocity never exceeded about $\frac{1}{6}$ of the synchronous field velocity. The region explored covered magnetic Reynolds numbers

$$R_m = \mu_0 \sigma \bar{V} R = (2\bar{V}R/\omega d^2) \leqslant 0{\cdot}25.$$

Hartmann numbers Ha, defined by $Ha = B_0 R(\sigma/\eta)^{\frac{1}{2}}$, ranged up to about 90, and the homochronous number $H_c = \Omega/\omega$ up to 0·2. Here σ = conductivity of mercury, $\bar{V}$ = flow velocity, R = cylinder radius, r = radial co-ordinate, $d = (2/\mu_0 \sigma \omega)^{\frac{1}{2}}$ = skin depth in mercury, ω = angular frequency of field and $\Omega = \bar{V}/r$.

2. Apparatus and method

2.1. *MHD system*

In a completely filled closed chamber the boundary conditions for fluid flow are simplified: surface waves are eliminated. Unpredictable variations in thermal impedance between the surface of insulated hot-film probes and the liquid metal have been a troublesome feature in previous studies of mercury flow and are usually attributed to fouling. Sajben's (1965) method of compensation can only be relied upon if fouling is constant during the course of each experimental run, and Hoff's (1969) method of reducing the effects of fouling by an amalgamated metal coating permits only shorter runs. These considerations led to the apparatus design shown in figure 1, where, for the sake of cleanliness, the closed system could be evacuated and transfer of mercury between the MHD chamber and reservoir accomplished by differential gas pressure. The main constructional material in contact with the mercury is stainless steel, but small amounts of 'Teflon', Neoprene and epoxy adhesive occur respectively in valves, gaskets and probes. Temperature variations are reduced by a water-cooled jacket around the cylindrical surface of the chamber. The chamber has an internal length $2L = 216$ mm and internal diameter $2R = 224$ mm.

The stator windings and core were taken from a two-pole, three-phase, 50 Hz, 160 h.p. motor with a hole diameter of 285 mm and length 233 mm. Figure 2 gives a circuit diagram of the power feed system. Tests at 50 Hz with a small rotatable coil showed that the magnetic field perpendicular to the axis in the empty chamber was very nearly circularly polarized at all points on the axis.

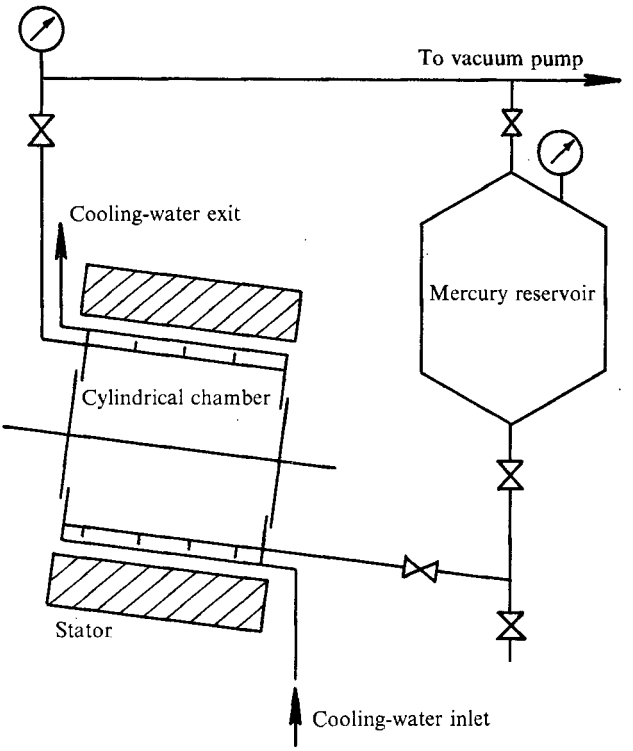

FIGURE 1. MHD system with mercury chamber and reservoir.

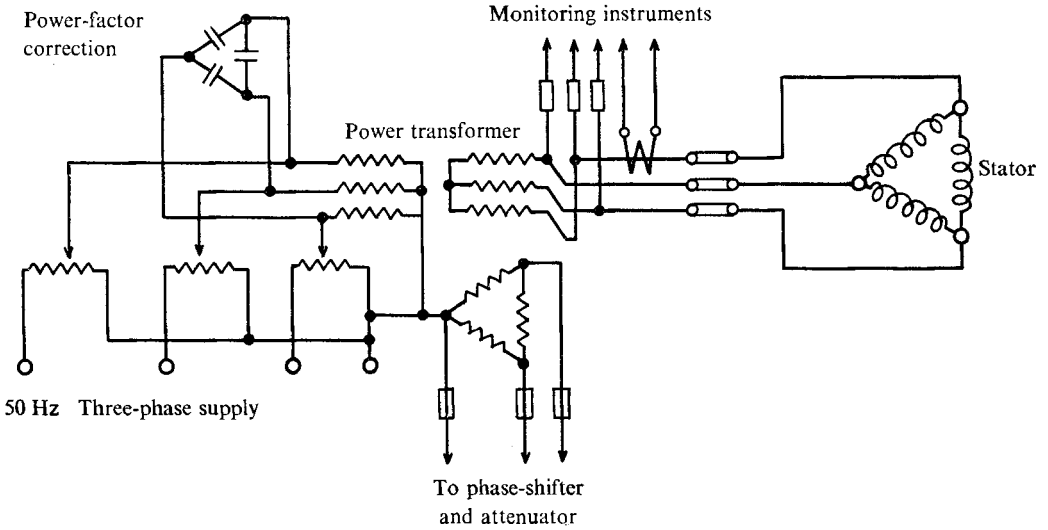

FIGURE 2. Circuit diagram.

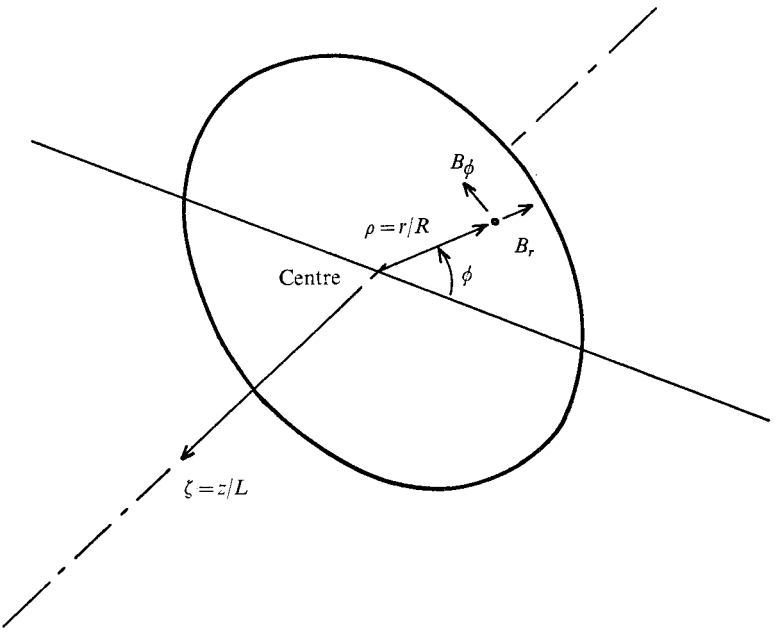

FIGURE 3. Cylindrical co-ordinate system (ρ, ϕ, ζ) with (0, 0, 0) at centre on chamber axis.

Near the cylindrical wall of the chamber some elliptical polarization was evident but the variation of the vector components throughout the enclosed volume was within $\pm 10\,\%$.

To facilitate reference to different points within the chamber, a system of polar co-ordinates (r, ϕ, z) has been adopted, based on the central point, as shown in figure 3. The dimensionless co-ordinates corresponding to r and z are $\rho = r/R$ and $\zeta = z/L$ respectively.

2.2. *Anemometric equipment*

For measurements in MHD systems with liquid metals, an ideal anemometer capable of indicating instantaneous values of the local magnitude and direction of the flow velocity at any point is still a distant goal. Metallic properties such as opacity, electrical conductivity, low Prandtl number and high density pose special problems, as does the presence of a varying magnetic field. In the absence of more suitable and promising new ideas for this type of anemometry it has been necessary in this work to press known techniques as far as possible and accept the limited accuracy and scope of the measurements. The main results pertain only to the dominant azimuthal (ϕ) velocity components and their validity is best judged in the light of the account in this and the next section of the problems arising and the solutions adopted.

The dominant azimuthal mean velocity component $\overline{V}$ was measured using a Pitot tube and a hot-film anemometer and the latter also yielded results for the r.m.s. fluctuating component $\tilde{v}$. A stainless-steel Pitot-static tube $\frac{1}{8}$ in. in

diameter† coupled to a simple mercury manometer provided mean velocity data in the higher ranges and was used in calibrating the quartz-insulated hot-film probes.‡ Hot platinum films were used, since strong disturbances due to magneto-resistance effects ruled out the more sensitive nickel films. To reduce variations in thermal impedance between the sensor and mercury, i.e. fouling effects, a very thin outer coating of non-amalgamating metal, vanadium, was evaporated onto the quartz. A high signal/disturbance ratio in liquid-metal MHD systems requires hot-film probe operation at relatively high power levels. The voltage drop along the length of the hot film appears also across the thin quartz film, with the result that small foreign particles might perturb the heat transport by being held electrostatically to the sensor surface. This possibility is obviated by the vanadium coating. The anemometer unit§ was used in the constant-temperature, or rather 'constant-overheat', mode to power the hot-film probe. This mode offers advantages as regards response time (Bradshaw 1971, pp. 88–89). A digital d.c. voltmeter and an r.m.s. voltmeter‖ with frequency response down to 1 Hz indicated the resulting bridge voltages E and $\tilde{e}$.

All hot-film measurements reported here were taken using conical probes (probe resistance $\sim 6{\cdot}5\,\Omega$, probe current $\sim 0{\cdot}25$ A in mercury). A diagram showing the sensor head dimensions is given in figure 4. Only a slight advantage in the form of faster response at high flow velocity would have attended the use of cylindrical probes. Such probes, without the vanadium outer coat, with length/diameter ratio about 20 were available, but as Hill & Sleicher (1971) have shown and our tests corroborated, this ratio is hardly enough to confer on them sufficient directional selectivity to merit a serious attempt at using them for mean and fluctuating velocity measurements in other than the ϕ direction. Furthermore, preliminary experiments showed them to be more susceptible to fouling, especially at high velocities. Normally the gas pressure over the mercury was 1 atm, but the vacuum facility was used to demonstrate two points of general interest, namely, that the heat transfer from a clean probe to the mercury was practically independent of the hydrostatic pressure and that neither the conical nor the cylindrical probes showed any sign of cavitation up to the highest flow velocities (about 2 m/s).

During most measurements two hot-film probes and one Pitot-static tube were mounted in the chamber. The former were adjustable to all values of r and z but the latter, apart from the rotation necessary to orient it to meet the flow at $\rho = r/R \approx 0{\cdot}5$, could be moved only along the z direction. Each hot-film probe was carried at the end of the leg of a stainless-steel T-shaped tube of diameter 4 mm. The tube arms passed through holes in the end walls of the chamber as shown in figure 5. Electric leads, twisted to minimize inductive pick-up, were taken out through the tubes. A drawback with this probe mounting is that it cannot maintain the conical sensor axis parallel to the local azimuthal flow in the cylinder. To minimize this error the leg of the T was kinked so that

† Type PCC-12-KL manufactured by the United Sensor Corp. (Watertown, Mass.).
‡ Supplied by Thermo-Systems Inc. (St Pauls, Minnesota).
§ DISA (Herlav, Denmark) type 55D01.
‖ DISA model 55D35.

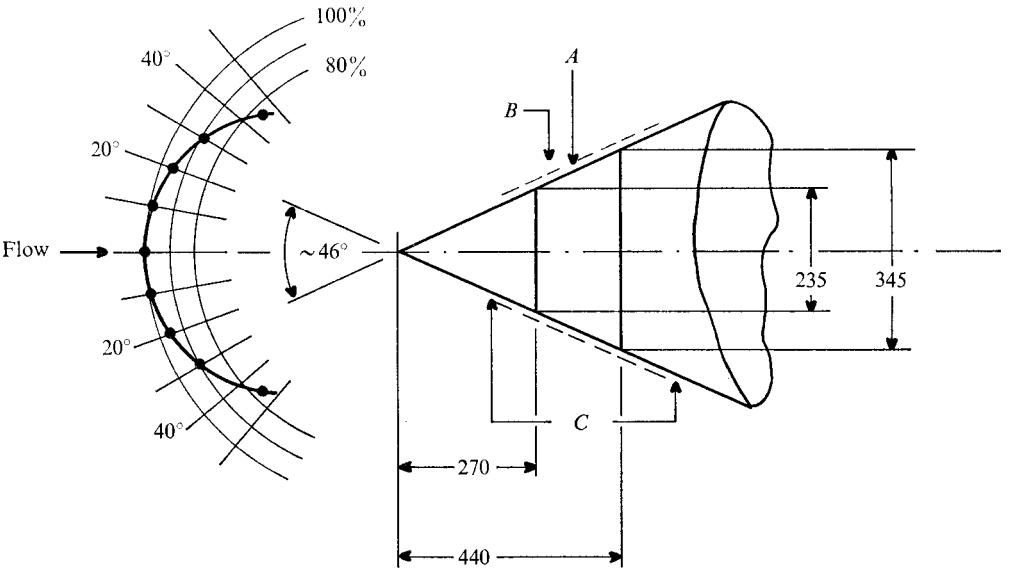

FIGURE 4. Probe sensor and polar response curve at 0·85 m/s. *A*, platinum film; *B*, quartz insulating film with vanadium outer coating; *C*, quartz substrate. Dimensions in μm.

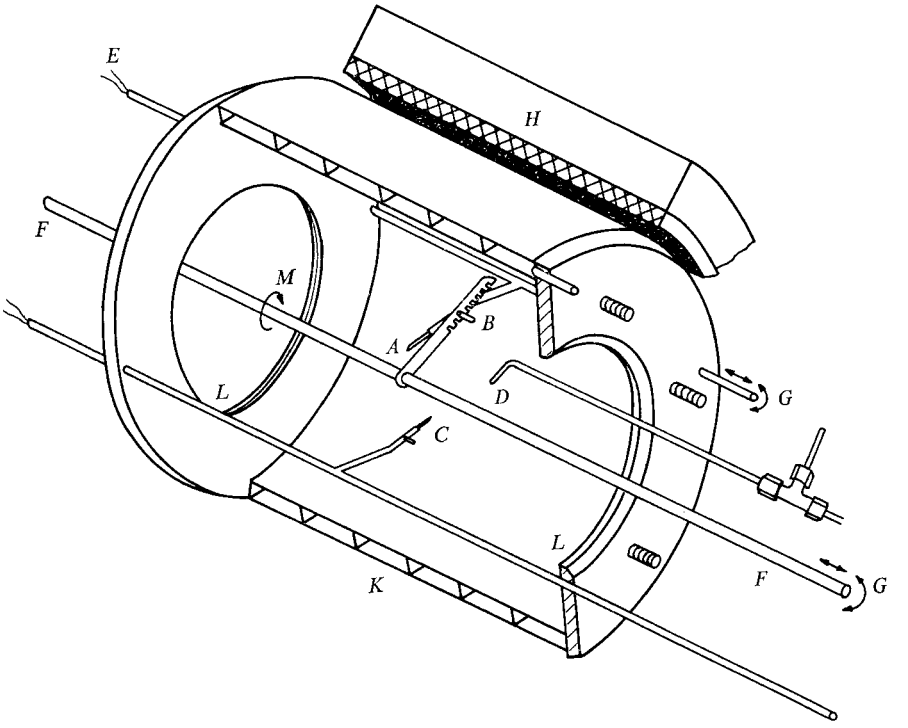

FIGURE 5. Sectional view of chamber showing probe mounting system, Pitot tube etc. *A*, probe 1; *B*, locking device; *C*, probe 2; *D*, Pitot-static tube; *E*, probe leads; *F*, 5 mm O.D. axial tube; *G*, probe positioning; *H*, stator; *K*, cooling jacket; *L*, end-wall ports; *M*, direction of fluid rotation.

the correct condition was obtained at the middle radius $\rho = 0{\cdot}5$. Figure 4 shows the mean velocity polar sensitivity curve for the probe at $\bar{V} = 0{\cdot}85$ m/s. Over the whole velocity range the sensitivity varied by less than $\pm 6\,\%$ for a $\pm 25\,^\circ$ flow deviation from the probe axis.

The strong hydrodynamical forces acting on any obstacle to flow in mercury pose special problems regarding the mechanical stability of probes and mounting systems. To achieve this stability a compromise had to be made. The hot-film probe actually in use was given additional support by locking a tag on its arm into one of a line of notches in a thin but stiff member fixed to a straight stainless-steel tube, O.D. 5 mm, passing coaxially right through the chamber and adjustable in the z direction so as to suit the desired z co-ordinate of the probe. Again, figure 5 shows the arrangement.

2.3. *Factors affecting anemometric accuracy*

Although there is no reason to believe that more refined studies will appreciably modify the basic quantitative results reached in this work, it would be a serious omission to gloss over a number of further questions pertaining to the truth and accuracy of the measurements. The following critical comments deal briefly with the most important of these questions.

2.3.1. *Hot-film probe calibration.* At low velocity ($< 0{\cdot}25$ m/s) probe calibration was carried out using mercury in an open annular channel which rotated steadily about a vertical axis. The channel had O.D. = 305 mm, I.D. = 242 mm and a mercury depth ~ 50 mm. Allowance was made for the mean slip between the mercury and the channel by counting electromagnetically the rotations of a tiny fragment of a permanent magnet rotating with and floating on the mercury surface. The probe blocks a certain cross-section of the channel, but there is a compensating effect due to a slightly increased depth of mercury near the probe, on account of the stationary wave it sets up in the channel. Correction for both these effects was made in deducing the mean flow velocity at the probe from the mean velocity of the magnetic float. The validity of this procedure was checked at higher velocities ($0{\cdot}25 < V < 0{\cdot}6$ m/s) with the Pitot-static tube in the channel, instead of the hot-film probe.

At velocities above 0·25 m/s the hot-film probes were calibrated in the actual chamber against the Pitot-static tube and manometer. With the Pitot tube at $\rho = 0{\cdot}5$, $\zeta = 0{\cdot}5$, the hot-film probe under calibration was set at the symmetrical point $\rho = 0{\cdot}5$, $\zeta = -0{\cdot}5$, the mean azimuthal velocities at these points being assumed equal. The idle hot-film probe was generally set at the mid-plane $\zeta = 0$ and at $\rho = 0{\cdot}5$. According to Hunt & Malcolm (1968) the Pitot-static tube pressure difference in a magnetic field perpendicular to the flow is given by

$$\Delta p = \tfrac{1}{2}\gamma V^2(1 + \alpha\sigma B^2 s/\gamma\bar{V}), \tag{1}$$

where γ = density of mercury, α = empirically determined constant of order 1 and s = Pitot-tube diameter.

In the present case, the parameter $\sigma B^2 s/\gamma\bar{V}$ in the bracketed correction was never greater than 10^{-3}; hence a simplified equation without the correction was used. Similar reasoning justifies neglect of the influence of the magnetic field on

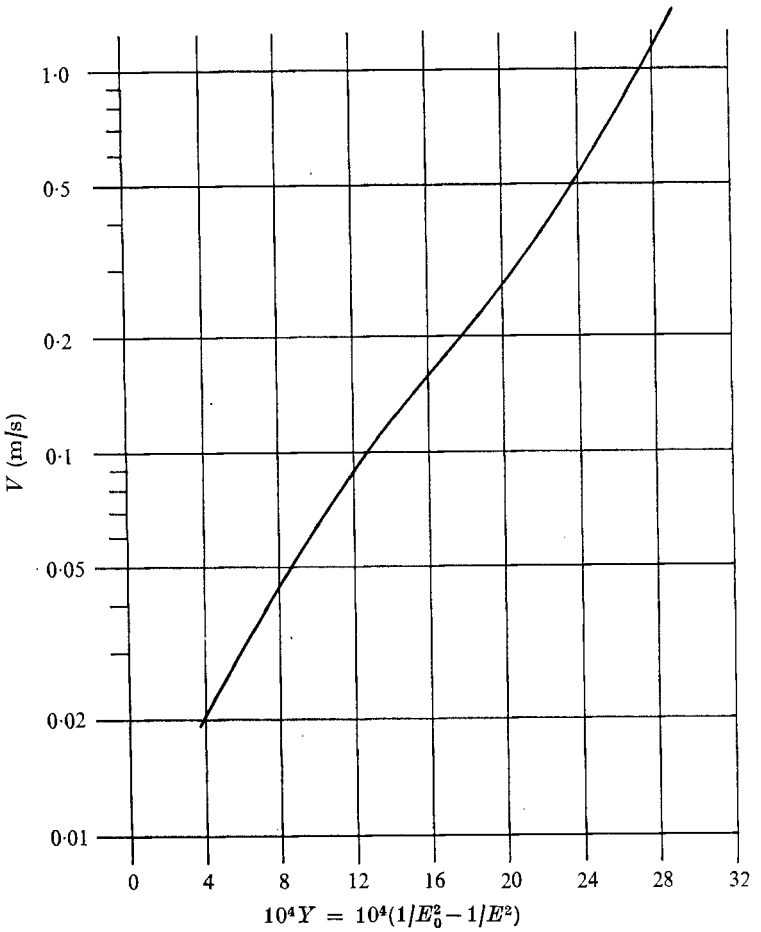

FIGURE 6. Typical hot-film probe calibration curve. $\overline{V}$ = mean flow velocity, E and E_0 mean bridge voltages with and without flow, respectively.

heat transfer from the hot-film probe (Malcolm 1969*a*). Besides the solenoidal $j \times B$ forces on the fluid there are irrotational $j \times B$ contributions equivalent to a pressure gradient having both mean and 100 Hz periodic parts. Neither of these should produce any signal at the Pitot manometers because the stagnation and static pressure sensing openings lie substantially at the same ρ and ζ co-ordinates, where, by symmetry, these pressures should be equal in amplitude. The manometers are too sluggish to respond to the phase difference in the periodic part. For turbulence intensities less than 10 %, Ower & Pankhurst (1966) estimate Pitot-static-tube mean velocity errors less than 2·5 %.

The calibration procedure resulted in a relation between the bridge voltage E and mean mercury velocity $\overline{V}$ for a given probe and overheat ratio. In this clean system small changes in heat transfer at $\overline{V} = 0$, ascribable to fouling, never exceeded $\pm 2{\cdot}5$ %. To cancel them we follow Sajben (1965) and evaluate the function

$$Y = 1/E_0^2 - 1/E^2, \tag{2}$$

where E_0 is the bridge voltage at zero flow. For convenience in evaluating turbulence, Y was usually plotted against $\ln \overline{V}$, such a curve being shown in figure 6.

2.3.2. *Disturbance from induced e.m.f.* Bednarz (1970), in studying MHD flows in a.c. induction furnace models, used hot-film probes, but made no mention of disturbances due to induced e.m.f. in the probe circuit. However, he employed the constant-current mode and was less interested in turbulence.

Here, it was found impossible to reduce the 50 Hz induced e.m.f. in the hot-film probe circuit to a satisfactorily low value merely by optimum disposition of the leads. Using a theory developed by Perry & Morrison (1971) an expression can be derived for the output signal across the bridge due to a disturbing signal in a constant-temperature anemometer, but their theory applies to an anemometer in a gas: in a low Prandtl number liquid the situation is somewhat more complicated owing to the influence of the fluid on the anemometer time constant. In the present apparatus it was found that the disturbance in the bridge output signal was several hundred times the induced e.m.f. in the probe circuit, which explains why it was necessary to take special steps to cancel this induced e.m.f. very accurately. Accordingly, a small unit incorporating an attenuator and phase-shifting transformer, fed from the same source as the stator coils, was connected so as to feed a compensating voltage into the bridge circuit. In the DISA model 55D01 this is easily arranged by feeding the compensating signal directly into a coaxial contact labelled 'test signal in' at the back of the anemometer. The adjustment procedure was to run the anemometer at very low overheat, so that turbulence gave only a small random signal on an oscillograph connected to indicate the bridge voltage. Thus, by observing the oscillograph, it was easy to adjust the phase and amplitude from the compensating unit so as to annul the 50 Hz disturbance practically to within the inherent noise across the anemometer bridge at zero flow, viz. 1–2 mV r.m.s. Then the overheat could be switched up to its normal value, which in these experiments was of order 15–20 °C. Because of system linearity, one such adjustment held over a fair range of magnetic field strengths, but it was necessary, of course, to readjust for each new probe position. An important deduction follows from the fact that adjustment for compensation could be made to within 1–2 mV: the magnetic field fluctuations which necessarily accompany turbulence in MHD systems were too small to perturb, by e.m. induction, these hot-film probe turbulence observations. The need for this check does not appear to have been realized in previous work with hot-film anemometers in MHD systems.

2.3.3. *Effect of probe supports.* In an otherwise rotationally symmetric chamber the drag on probes and supports may be expected to influence the flow to a measurable degree. To investigate this influence, a series of measurements was made in which the hot-film probes and Pitot tubes were removed one at a time, thus approaching the geometry of the bare cylinder. Measurements of mean velocity (to be reported in detail elsewhere) were also performed with a special, relatively drag-free, rotating-vane anemometer pivoted on the chamber axis. The magnitude of the effects due to probe drag will be made clear in the later section on quantitative results. Moving a probe to a new position leads to changes

in the velocity at another fixed probe. In the present apparatus these changes did not exceed $\pm 7\,\%$.

Measurements at radii less than $\rho = 0{\cdot}2$ were not made on account of the difficulty in interpretation of hot-film anemometer signals at high turbulence intensities. In a rotating flow, a probe can be said to lie directly in its own wake. By moving one probe past the same ζ co-ordinate as the other, but with a ϕ difference of 180° it was possible to show that mean velocity and turbulence were only weakly affected by this local own-wake effect.

2.3.4. *Turbulence evaluation.* Since no general account of the response of these hot-film probes in liquid metals appears to have been published, it will be necessary to indicate how response characteristics may have influenced the present measurements.

One clear limitation is set by the probe size, which, according to figure 4, is seen to be of order $250\,\mu$m; the response to eddies smaller than this will certainly be attenuated. Dimensional comparison may be made with the length l_l characterizing the energy-containing eddies, and with the Kolmogorov length η, characterizing the energy-dissipating eddies in isotropic turbulence. Hinze (1959) defines these as

$$l_l \sim \tilde{v}^3/\epsilon, \quad \eta \sim (\nu^3/\epsilon)^{\frac{1}{4}}, \tag{3), (4}$$

where ϵ = turbulent energy dissipation rate per unit mass and ν = kinematic viscosity of mercury ($\sim 10^{-7}\,\mathrm{m^2\,s^{-1}}$). For the strongest magnetic fields used in these measurements, the mean value of ϵ, calculated by a rough integration over the chamber volume of the product of the MHD force and the local mean flow velocity $\overline{V}$ was about 4 W/kg. The r.m.s. velocity fluctuation $\tilde{v}$ was then about 0·1 m/s. Hence l_l was of order $250\,\mu$m and η of order $4\,\mu$m. Now $\tilde{v}$ was found to be roughly proportional to B and ϵ to B^3, so that l_l is independent of B and η varies as $1/B^{\frac{3}{4}}$. It is therefore apparent that the probe size may allow fair response to the main part of the energy-containing eddies, but not to the energy-dissipating eddies.

A simplification which has been accepted in this work is the use of the steady-state calibration of the bridge voltage against the mercury velocity in estimating the turbulent velocity component. A simple evaluation of turbulence intensity is then possible using Malcolm's (1969*b*) formula, which, in the present notation, gives the turbulent intensity as

$$\tilde{v}/\overline{V} = 2S\tilde{e}/E^3, \tag{5}$$

where $\tilde{e}$ = r.m.s. bridge voltage, E = d.c. bridge voltage and $S = d\ln V/dY$ = slope of steady-state probe calibration curve as shown, for example, in figure 6.

Experimental calibration of the probe with an oscillating flow would constitute a more satisfactory assurance of validity, but is considered sufficiently difficult to warrant a separate study. The arguments about to be presented seem to provide justification for the procedure adopted.

A finite response time of the anemometer leads to a sacrifice of accuracy at higher fluctuation frequencies in the turbulence spectrum. To include the main energy-containing eddies this time should be sufficiently short for eddy sizes down to $\frac{1}{4}$ mm so the response time at the highest magnetic field (where $\overline{V} \approx 2$ m/s)

need be no shorter than $\tau = \frac{1}{8} \times 10^{-3}$, i.e. 125μs. At the weakest field, which was about 50 times smaller, $\tau \approx 6$ ms would be acceptable. These maximum response times correspond to minimum response frequencies of 4000 and 80 Hz respectively. In modern constant-temperature hot-film anemometers the servo-loop amplifier transconductance (~ 12 A/V) is high over a wide bandwidth (~ 100 kHz), which implies that transient departure of the film temperature from the demanded constant value is, at any rate in these experiments, not a main factor in limiting response. Although only a sketch of the arguments, the following section has the threefold aim of revealing what the important factors are, of explaining why the conventional method of response-time checking is not valid and finally, of providing theoretical evidence for the adequacy of the true response time of these probes in the present measurements.

2.3.5. *Probe response time.* Steady-state calibration of a probe should ideally be carried out in a uniformly streaming fluid moving at a steady velocity. In a turbulent flow the hot-film temperature and the instantaneous local streaming velocity may be the same as in a steady-state calibration, but generally the instantaneous heat fluxes from the probe will differ. The difference is clearly associated with the different distributions of temperature and velocity. However, use of the steady-state calibration in estimating the instantaneous local streaming velocity is acceptable if the velocity and temperature distributions in the two cases are sufficiently similar in a rather limited region around the actual sensor. The error in using the steady-state calibration may therefore be ascribed to two effects. The first is purely hydrodynamical, and is concerned with the time required for the boundary-layer flow around the sensor to adjust to the local mainstream flow. Lighthill (1954) has shown that this time is small: for a flat plate it has a negative value, becoming a 'time of anticipation' of the order of a fraction of $x'/\overline{V}$, where x' is the plate length parallel to the flow. The second effect is concerned with the time required for the temperature distribution to adjust to the local flow changes; or, in other words, the time required for the isothermal contours to take up a new configuration. It is just this time which, one hopes, could be measured by the simple conventional method of studying the response of the probe in the flowing fluid to an applied small change in probe temperature of either square-wave or variable-frequency sinusoidal form. For this method to be valid it is necessary to know the temperature variation at the actual probe–mercury interface and the variation of the heat flux which passes through this surface into the mercury. With presently available probes in liquid-metal flows it is contended that neither of these two quantities is accessible to proper measurement by the conventional method. What the method does give is the relation between the hot-film temperature and the heat flux from the film itself. Experiments have shown that the main causes of divergence between these latter and the former quantities arise from (i) a considerable capacitive heat flux flowing from the film into the conical quartz substrate and (ii) a considerable temperature fall, at higher flow velocities well over 50 % of the total, which occurs in the thin quartz insulating coat between the hot-film and the mercury. (It should be noted that this high temperature fall does not imply that the coating itself contributes appreciably to thermal delay: Malcolm's

(1969*b*) estimate of its inherent time constant, 10^{-5} s, cannot be far out.) Subsidiary experimental means of acquiring the data needed to estimate the unknown pair of quantities from the measured pair are less appealing than the separate project of probe calibration in an oscillating flow. Here, we take the still easier course of demonstrating the adequacy of our probe response time by providing an order-of-magnitude theoretical estimate of its value.

Consistent with ordinary response-time of bandwidth arguments, in still mercury we may take the region of main thermal gradient as extending to a distance p from the probe surface where the temperature excess is about $\frac{1}{3}$ that at the surface. Treating the probe as a spherical object of radius $\sim 150\,\mu$m gives this distance p as $300\,\mu$m from the surface. The probe response to a sinusoidal probe temperature variation of frequency f will be a satisfactory approximation to the response when $f \to 0$ if the wavelength λ of the thermal conduction waves emitted by the probe is several times this distance p. If we take $\lambda = 4p = 1200\,\mu$m, we find from $\lambda^2 = 4\pi\kappa/f$ (where κ = thermal diffusivity of mercury) a response frequency $f_r = \pi\kappa/4p^2 \approx 35$ Hz. It is in still mercury that the errors of the conventional method, as discussed above, are least and it is therefore not surprising that such measurements gave a similar value, namely $f_r \approx 20$ Hz for a 3 db fall relative to $f \to 0$.

For sufficiently small flow velocities the isotherm at $\frac{1}{3}$ of the excess temperature is scarcely modified and the frequency response will still be given by

$$f_r \approx 4\pi\kappa/\lambda^2 = \pi\kappa/4p^2.$$

At somewhat higher flow velocities, deformation of this isotherm sets in and permits a lower λ and higher f value. In this velocity range the limit of f ensuring that the heat flux–probe temperature relation changes only mildly with increases of f upwards from zero can be seen to be that the thermal waves associated with frequency f propagate from the probe no faster than $\bar{V}$, the flow velocity. The quoted condition on the thermal wave velocity limits the capacitive heat flow associated with the sinusoidal probe temperature component, and leads to a frequency response f_r given by

$$f_r \approx \bar{V}^2/4\pi\kappa. \tag{6}$$

At $\bar{V} = 5$ cm/s in mercury $f_r \approx 55$ Hz and at $\bar{V} = 15$ cm/s, $f_r \approx 500$ Hz. Equation (6) becomes invalid when the thermal wavelength becomes smaller than the sensor dimensions. The new condition which now determines the response frequency is that the thermal wavelength be several times δ_κ, the thickness of the thermal boundary layer. From the relation given by Schlichting (1968) for flow past a flat plate, the thickness of the thermal boundary layer in a low Prandtl number fluid is given by

$$\delta_\kappa \approx \tfrac{4}{3}[\kappa x'/\bar{V}]^{\frac{1}{2}}, \tag{7}$$

where x' is distance along the hot plate. If we take $\lambda \approx 4\delta_\kappa$ the result for f_r becomes

$$f_r \approx 9\pi\bar{V}/64x'. \tag{8}$$

A glance at the conical probe design in figure 4 reveals a complication. The viscous boundary layer will grow right from the apex of the cone and will already

have reached a finite thickness before the flow reaches the hot-film region. Rough calculation shows that, despite the handicap, the thermal boundary layer just about succeeds in penetrating the viscous boundary layer. The consequence will be a slightly lower f_r than that given in the above equation (8). Inserting typical values in this equation with $x' = 180\,\mu$m results in $f_r \approx 750$ Hz at $\overline{V} = 30$ cm/s and $f_r \approx 5000$ Hz at $\overline{V} = 2$ m/s.

The low thermal conductivity of the conical quartz substrate compared with that of mercury should exclude the type of high-frequency fall in sensitivity discussed by Bellhouse & Schultz (1967) in connexion with anemometry in gases.

From the above it is seen that the conical probes used were just adequate for measurements of turbulence down to eddies of size about l_l, and that the steady-state calibration relating the bridge voltage to the mean velocity should hold even for the corresponding turbulent velocities.

2.3.6. *Fluid temperature fluctuations.* Simple evaluation of turbulence intensity using thermal anemometers in fluid systems presupposes that the probe response to velocity fluctuations far exceeds that due to any temperature fluctuations which may be present (Bradshaw 1971). In MHD systems it is of particular importance to ascertain whether this condition holds because of the dissipation of Joule heat in the fluid. Running the probe at increasing overheat temperatures θ causes the ratio $\tilde{e}/E$ to tend to a constant value for which the effects of temperature fluctuations are negligible. The decision to fix θ at about 20 °C in this work was reached as a compromise after studying the form of such curves relating $\tilde{e}/E$ to overheat and paying regard to the detrimental effects of very high probe power dissipation on probe life.

For any fixed point in the chamber, measured values of $\tilde{e}/E$ when plotted against $1/\theta$ were found to lie close to a straight line whose slope was a function of ρ and ζ. The absolute value of the slope increased at higher magnetic fields. Accordingly a correction factor was applied to the right-hand side of (5) by taking observations of $\tilde{e}/E$ for varying θ up to $\theta \approx 20$ °C and extrapolating along the line to $\theta \to \infty$, where $\tilde{e}/E$ is unaffected by temperature fluctuations. For magnetic fields B_0 below 10 mT the correction was trivial, the factor being approximately 1·0. At $B_0 = 30$ mT (as in the turbulence data of figures 10 and 12) the correction factor varied at different points from 0·78 to 1·07. At the highest magnetic field $B_0 = 53$ mT values of the correction factor as low as 0·43 were noted. Further increases of B_0 would thwart the use of hot-film probes in the study of turbulent velocity.

2.4. *Magnetometry*

Preliminary tests showed that the form of the magnetic field variation at points within the mercury in the chamber was practically independent of the stator-coil magnetizing current I. Observations of the magnetic field at its highest values from the moment of application of the magnetizing current until the attainment of steady mean flow revealed a change of at most 1·3 % in the effective field as the mercury flow built up: the field behaved practically as if the mercury were a stationary solid conductor. Under these conditions and with full axial

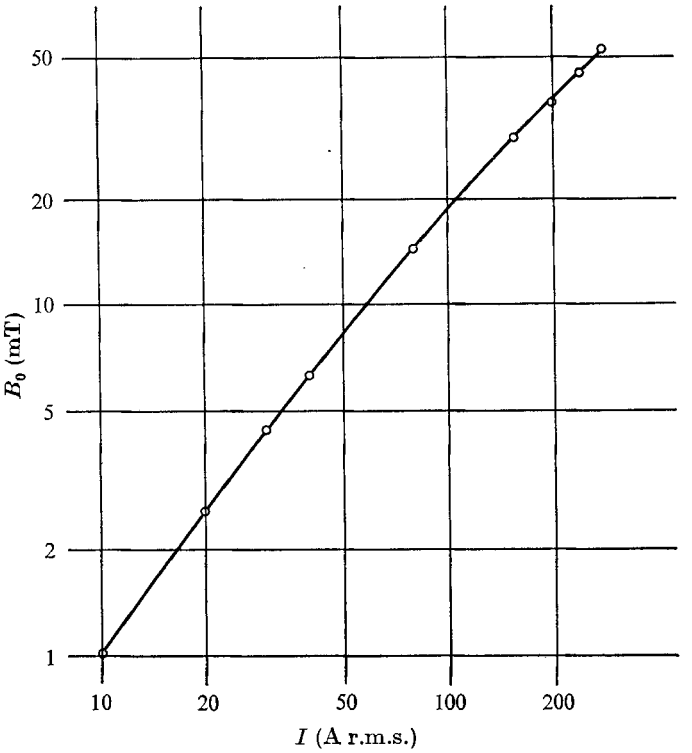

FIGURE 7. Amplitude of circularly polarized magnetic field B_0 on axis at centre of mercury-filled chamber, as function of stator current I.

symmetry, the field components B_r, B_ϕ and B_0 at any point (ρ, ϕ, ζ) within the mercury can be expressed as

$$B_r = B_0 f(\rho, \zeta) \sin(\omega t - h + \phi), \tag{9a}$$

$$B_\phi = B_0 g(\rho, \zeta) \sin(\omega t - k + \phi), \tag{9b}$$

$$B_z = B_0 m(\rho, \zeta) \sin(\omega t - n + \phi), \tag{9c}$$

where B_0, the field amplitude within the mercury at $\rho = 0$, $\zeta = 0$, is a function of stator coil current I, ω, the angular frequency of power supply, is $314\,\mathrm{s}^{-1}$ and f, g, m, h, k and n are functions of (ρ, ζ). Several checks showed that the field was very nearly symmetrical about the plane $\zeta = 0$, i.e. m is odd and f, g, h, k and n are even.

The object of the magnetometry was to obtain a first approximation to the various mean MHD forces by calculation from measurements of f, g, m, h, k and n at a number of points in the fluid and by measurement of B_0 as a function I. Figure 7 shows the relation between B_0 and I.

The field distribution was investigated using magnetic field sensors† consisting of three small concentric mutually perpendicular 100 turn coils fully

† Supplied by Southern Measuring Instruments Ltd., Chislehurst, England.

ζ	ρ	f	g	m	h (deg)	k (deg)	n (deg)
0	0	1·00	1·00	0	−90	0	—
0	0·4	1·00	1·00	0	−86	10	—
0	0·8	1·08	1·06	0	−72	39	—
0	0·96	1·19	1·20	0	−59·5	61	—
±0·5	0	0·94	0·94	0	−77·5	12·5	—
±0·5	0·4	0·98	0·97	∓0·07	−75·5	21	−34
±0·5	0·8	1·11	1 06	∓0·125	−58·5	43	−19
±0·5	0·96	1·23	1·15	∓0·145	−52·5	62·5	−13
±0·8	0	0·93	0·93	0	−55	35	—
±0·8	0·4	0·97	0·97	∓0·12	−54	37	−44
±0·8	0·8	1·16	1·07	∓0·25	−47	48	−22
±0·8	0·96	1·34	1·11	∓0·30	−40	59·5	−13

TABLE 1. The phases h, k and n and relative amplitudes f, g and m of 50 Hz field components at the point (ρ, ϕ, ζ) within mercury-filled chamber

insulated against the mercury by an epoxy encapsulation of size 6·5 × 6·5 × 8 mm. Measurements were made with the chamber full of mercury at points (ρ, ζ) given by $\rho = r/R = 0$, ±0·4, ±0·8 and ±0·96; $\zeta = z/L = 0$, ±0·5 and ±0·8. A field survey, carried out at $I = 120$ A, gave the results in table 1.

2.5. *Estimation of MHD forces*

At any point in the chamber there will be three MHD force components given by

$$F_r = -j_z B_\phi + j_\phi B_z, \tag{10a}$$

$$F_\phi = j_z B_r - j_r B_z, \tag{10b}$$

$$F_z = -j_\phi B_r + j_r B_\phi. \tag{10c}$$

Although the fields were measured the current densities were not, but they can be obtained via Maxwell's equation, $\operatorname{curl} B = \mu_0 j$, which leads to

$$j_r = \frac{1}{\mu_0}\left[\frac{1}{r}\frac{\partial B_z}{\partial \phi} - \frac{\partial B_\phi}{\partial z}\right], \tag{11a}$$

$$j_\phi = \frac{1}{\mu_0}\left[\frac{\partial B_r}{\partial z} - \frac{\partial B_z}{\partial r}\right], \tag{11b}$$

$$j_z = \frac{1}{\mu_0}\left[\frac{\partial B_\phi}{\partial r} + \frac{B_\phi}{r} - \frac{1}{r}\left(\frac{\partial B_r}{\partial \phi}\right)\right]. \tag{11c}$$

The amplitudes and phases of all the above partial differential coefficients were estimated from those of B_r, B_ϕ and B_z in table 1, and the various products were calculated graphically. The results giving the values of the expressions $\mu_0 \bar{F}/B_0^2$, corresponding to each of the mean force components, are shown in figure 8. An absolute accuracy better than ± 25 % cannot be claimed. Values of $\mu_0 \bar{F}_\phi/B_0^2$ and $\mu_0 \bar{F}_r/B_0^2$ calculated using Dahlberg's (1972) theory, which applies to an infinitely long cylinder, are shown in parentheses. Some of the differences between the theory and measurements seem too great to be ascribed solely to inaccuracy of the latter and must be partly due to the difference in length.

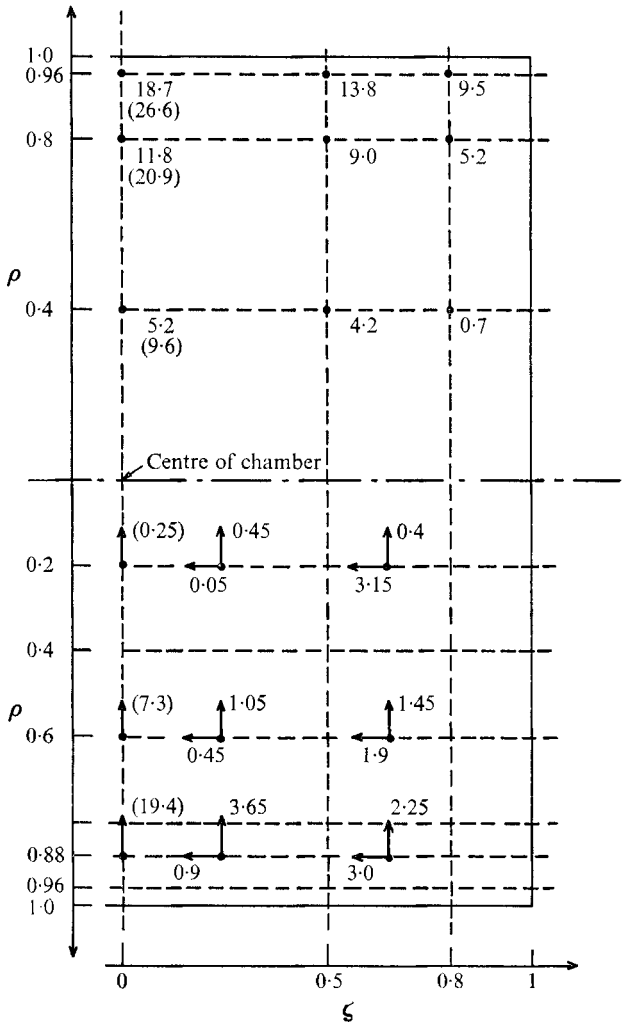

FIGURE 8. Mean MHD force $\bar{F}_\phi$, $\bar{F}_r$ and $\bar{F}_z$ per unit volume acting at indicated points on mercury in chamber. Upper part of diagram gives magnitude of $\mu_0\bar{F}_\phi/B_0^2$; lower part gives magnitudes and directions of $\mu_0\bar{F}_r/B_0^2$ and $\mu_0\bar{F}_z/B_0^2$. In parentheses, theoretical values of $\mu_0\bar{F}_\phi/B_0^2$ and $\mu_0\bar{F}_r/B_0^2$ for an infinitely long chamber are given. Units are m^{-1}.

Several spectral analyses of the turbulent fluctuations were carried out, but none showed any sharp 'hump' at 100 Hz or elsewhere. It is therefore concluded that the influence of the periodic MHD forces on flow and turbulence under the present conditions is negligible.

3. Results and discussion

3.1. *Mean flow and turbulence*

Figure 9 shows results from a series of measurements of the mean velocity $\bar{V}$ at different points within the chamber, for three different magnetic field strengths. The corresponding results for the r.m.s. turbulent velocity $\tilde{v}$ are shown in

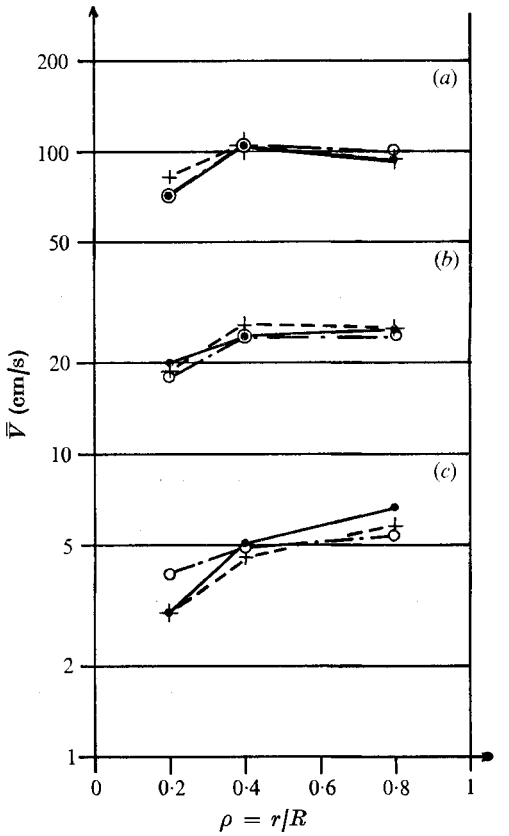

FIGURE 9. Mean rotational velocity $\overline{V}$ at various points in chamber for three magnetic field strengths: (*a*) $B_0 = 30\,\mathrm{mT}$, (*b*) $B_0 = 6{\cdot}3\,\mathrm{mT}$, (*c*) $B_0 = 1\,\mathrm{mT}$. —●—●—, $\zeta = 0$; – –○– –○– –, $\zeta = \pm 0{\cdot}5$; - - -+- - -+- - -, $\zeta = \pm 0{\cdot}8$.

figure 10. Despite the combined effects of a strong fall-off in the MHD driving force and the extra resistance to flow near the end walls of the chamber, the variation of flow with ζ is very small. It is as if the driving and frictional forces averaged along the chamber produce a mean flow, almost independent of the ζ co-ordinate.

Variation of the flow with radius is illustrated by the series of measurements summarized in the curves of figure 11, which give values averaged over the three ζ co-ordinates 0, 0·5 and 0·8. The curves show the mean angular velocity $\Omega = \overline{V}/r$ of the flow at different radii r and for magnetic field strengths B_0 from 1 to 53 mT. It is evident that Ω is approximately proportional to B_0 and thus to $\overline{F}_\phi^{\frac{1}{2}}$. Had the flow been laminar Ω would have varied directly as $\overline{F}_\phi$. A rapid rise of Ω from zero in the vicinity of the wall is characteristic of a boundary layer around a region of turbulent flow.

3.2. *Effect of probe drag*

Figure 11 provides evidence concerning the influence of probe drag on the measurements. Angular velocity profiles with $B_0 = 6{\cdot}3$ and 30 mT are shown for

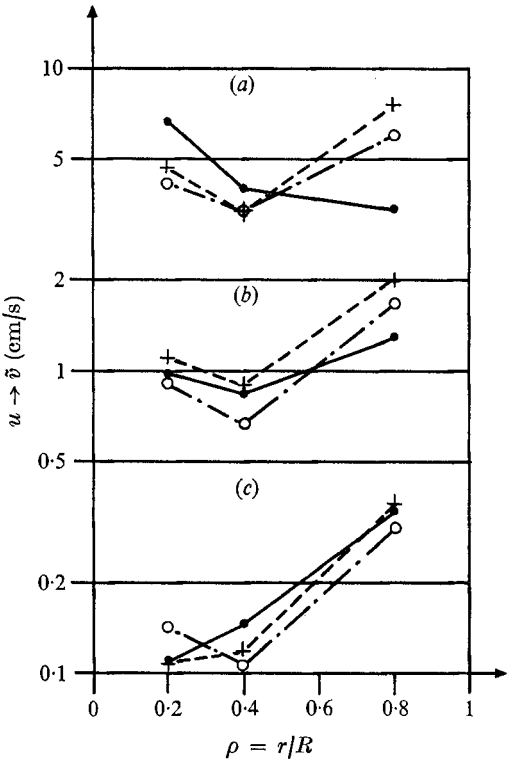

FIGURE 10. Turbulent velocity component $\tilde{v}$ in ϕ direction at various points in chamber for three magnetic field strengths: (*a*) $B_0 = 30\,\mathrm{mT}$, (*b*) $B_0 = 6{\cdot}3\,\mathrm{mT}$, (*c*) $B_0 = 1\,\mathrm{mT}$. —●—●—, $\zeta = 0$; – –●– – –●– –, $\zeta = \pm 0{\cdot}5$; · · ·●· · ·●· · ·, $\zeta = \pm 0{\cdot}8$.

the case when the redundant probe, at $\rho = \frac{1}{2}$, $\zeta = 0$, was completely removed from the chamber. Naturally the Ω profile lies higher, especially near the cylindrical wall, where the rise is about 20 %. This form of rise in the profile is to be expected since the main contribution to drag on the probe should be located on the T arms (see figure 5) rather than on the leg. Also shown in figure 11 are results from Pitot-tube observations at $\rho = 0{\cdot}5$ with only the one probe present: these imply similar profile rises. The Pitot tube was also used to measure the velocity at $\rho = 0{\cdot}5$, $\zeta = 0{\cdot}5$ when both probes were removed from the chamber. These results, too, are shown in figure 11: as expected they indicate a further velocity increase, this time by about 30 %. To approach more nearly the unimpeded flow in the cylinder a special minimum-drag anemometer was designed. It took the form of a rotating-vane device, pivoted on the axial tube through the chamber. Details of the construction are to be reported elsewhere. Two such devices were used, one at $\rho = 0{\cdot}3$, the other at $\rho = 0{\cdot}7$. When the Pitot tube and both probes were removed, these vane anemometers gave results which are also shown in figure 11. They confirm the decided slope of the Ω *vs.* r profile and, as expected, yield the highest values for a given field. Although figure 11 does not show it, they also confirmed the very weak dependence of Ω on ζ.

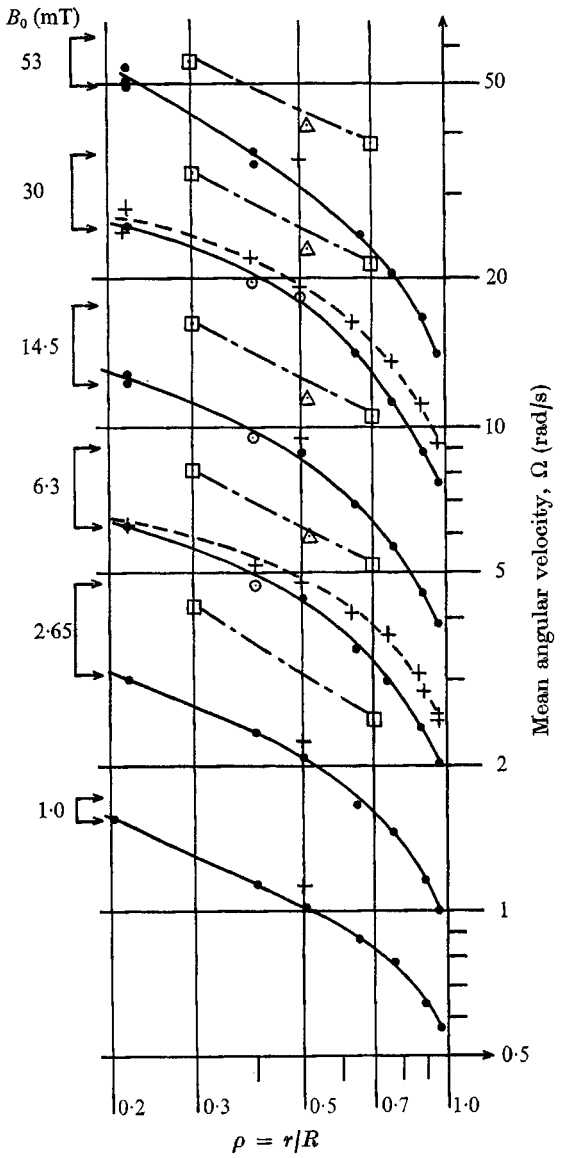

FIGURE 11. Mean angular rotational velocity Ω at various points in chamber for six magnetic field strengths. —●—●—, with two probes plus one Pitot-static tube; - - -+- - -+- - -, with one probe plus one Pitot-static tube; △, with Pitot-static tube only; —□— - —□—, with moving-vane anemometer only.

3.3. *Secondary flow*

Some of the properties peculiar to a rotating volume of fluid have been described by Greenspan (1968). He states that "rotating flows have a strong disposition towards two-dimensionality". It may be that the relatively weak dependence of angular velocity Ω on ζ (despite the ζ variation of $\overline{F}_\phi$ and the end-wall friction) is a manifestation of this tendency.

In this connexion an attempt was made to test for the existence of secondary flow in the chamber. Accordingly, a simple form of pulsed-wire anemometer, of the type described by Bradbury & Castro (1971), was placed at various points on the axis of the chamber. The 5 mm O.D. axial tube, the probes and Pitot tube were all removed for this particular investigation. Secondary flow should show up prominently on the axis,† since the primary flow $\overline{V}$ is slow there. Clear evidence was obtained for a mean flow parallel to the chamber axis and towards the centre from each end wall. The steady velocity varied roughly as B_0 but was quite small, being about 1·5 cm/s at $\zeta = \pm 0{\cdot}5$ for $B_0 = 30$ mT. This velocity is several times smaller than the mean value of $\tilde{v}$, the corresponding r.m.s. turbulent velocity. The distribution of radial and axial forces shown in figure 8 suggests that the secondary flow pattern may be more complicated than that of a single toroid in each half of the chamber.

3.4. *Calculation of flow and turbulence*

Computer calculations of the one-dimensional rotating flow in an infinitely long cylinder under the action of the experimentally determined mean MHD force have been carried out by a colleague, Mr Kjell Larsson (1973). His analysis is sketched in the appendix. Typical results are shown in figure 12, from which it is seen that there is fair agreement with the measured mean angular velocity. That the profile slopes less may be due to the absence of end-wall effects in the infinitely long cylinder. Figure 12 also shows that the turbulence intensity $\tilde{v}/V$ calculated is less than that measured. Examination of the wave form of the turbulent signal from the hot-film anemometers indicated one factor possibly responsible for this difference. Nearer the axis of the chamber there is an increasing component of very low frequency, which suggests that rotational flow of the fluid is about an axis parallel to the chamber axis but moving slowly around at a short distance from it. It does not appear that the magnetic field in these experiments is strong enough to have any profound direct effect on the turbulent motion itself.

3.5. *Power dissipation*

The greater part of the power dissipation in the liquid is due to Joule heating P_j by the induced currents. Next comes the power loss P_ε due to dissipation of turbulent energy. Experimentally, the total dissipation was measured by observing the heat transferred to the cooling water. At the highest magnetic field used ($B_0 = 53$ mT) this was about 2 kW. The power delivered to viscous dissipation could be calculated by integrating the e.m. power input to the flow alone over the whole chamber, i.e. by evaluating the integral

$$P_\varepsilon = \iiint \overline{V}\overline{F}_\phi r \, d\phi \, dr \, dz \approx 4\pi R^3 L \int_0^1 \rho^2 \overline{F}_\phi \Omega \, d\rho. \tag{12}$$

† A referee has pointed out that secondary flow is most likely to occur near the cylinder wall, i.e. in a region of adverse angular momentum distribution.

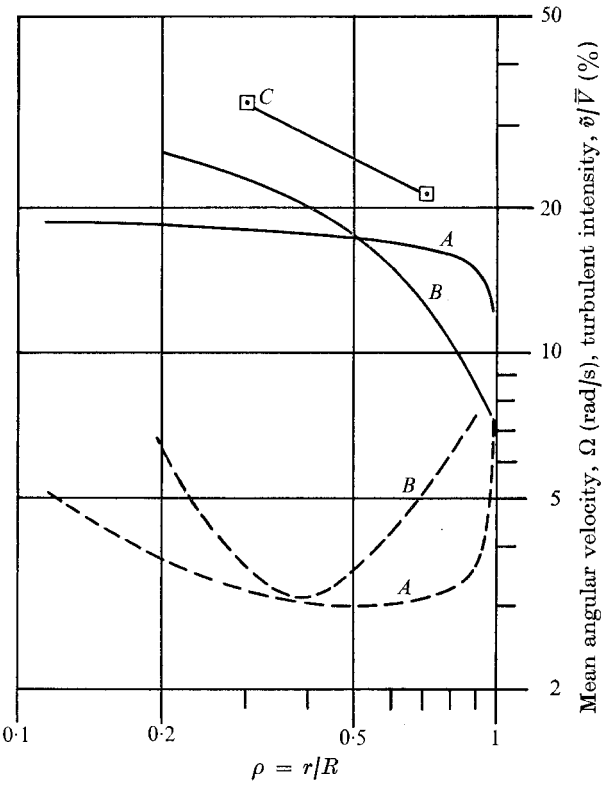

FIGURE 12. Mean angular rotational velocity Ω and turbulence intensity $\tilde{v}/\overline{V}$ at $B_0 = 30\,\mathrm{mT}$. ——, Mean angular velocity; – – –, turbulence intensity; *A*, theoretical values for infinite cylinder; *B*, values measured with two probes and one Pitot-static tube in chamber (means for $\zeta = 0$, $\pm 0{\cdot}5$ and $\pm 0{\cdot}8$); *C*, value of Ω with rotating-vane anemometer only in chamber.

A rough estimate of this power, under the same conditions as above gave the result $P_e \approx 440\,\mathrm{W}$, i.e. only about 14 % of the power was dissipated via turbulence. The value of ϵ used in § 2.3.4 is just P_e divided by the mass of mercury in the chamber.

3.6. *Scaling laws*

In metallurgical applications of MHD, dimensional analysis shows to what extent the behaviour of a large projected plant can be studied on a model scale. Ideal scaling requires that the value of each relevant dimensionless quantity be preserved. In the rotator we have four independent non-dimensional quantities, one combination being, for example: $Re = \overline{V}R/\nu$, S_u (the electromagnetic interaction parameter) $= \sigma B^2 R/\gamma\overline{V}$, Δ (the radius to skin depth ratio) $= (R^2\mu_0\sigma\omega/2)^{\frac{1}{2}}$ and $H_c = \Omega/\omega = \overline{V}/\omega R$. A dimensionless relation between these relates the seven variables $V, R, B, \omega, \gamma, \sigma$ and ν to one another. If media with the correct properties γ, σ and ν were available the main condition for ideal scaling would be satisfied. As this is generally not so, scaling is usually based on the assumption that one or more of the dimensionless groups may be allowed to diverge somewhat, between the model and full-scale situations. For example, if we assume that the

fluid motion is dominated by electromagnetic and inertial forces, we specify constant values for S_u, Δ and H_c but allow Re to change. We can now explore briefly scaling rules, e.g. for a rotator for molten steel n times the linear dimensions of the model. Variables for the full-scale device will be indicated by a prime. From data on γ, σ and ν for mercury and molten steel it can be shown that the equality conditions on S_u, Δ and H_c lead to the relations

$$\left.\begin{aligned} V' &= 2V/n, \quad \omega' = 2\omega/n, \quad B' = B(2/n)^{\frac{1}{2}}, \\ P'_j &= 4P_j/n, \quad P'_\varepsilon = 4P_\varepsilon/n, \quad Re' = \tfrac{1}{3}Re. \end{aligned}\right\} \tag{13}$$

It should be noted that the total powers P'_j and P'_ε decrease as n increases. Since larger devices are normally more powerful we see that the regime studied in this work, namely with small H_c, is of little value in scaling to a large high-powered device. For this latter purpose model studies at much higher powers with the homochronous number approaching unity would be required. It is also clear that problems with overheating prohibit modelling on too small a scale.

The author wishes to thank J. Braun (head, General Physics Section, AB Atomenergi) and several colleagues, E. Dahlberg, S. Linder, D. G. Malcolm and W. Ohlsson, for stimulating discussions and practical assistance in connexion with this work. Thanks are also due to the Directors, AB Atomenergi, Studsvik, and to the Swedish Board for Technical Development for financial support.

Appendix

By Kjell Larsson, AB Atomenergi, Studsvik, Fack, Nyköping, Sweden

The calculations are based on the empirical eddy-diffusivity method of Prandtl (1945) with modifications used by Kjellström (1972). In the stationary problem the conditions of symmetry and continuity in an infinitely long cylinder lead to zero axial and radial mean velocities and to z independence for Ω and q (the turbulence energy per unit mass).

The momentum equation is taken as

$$\frac{d}{dr}\left\{r(\mu+\gamma\epsilon_r^\Omega)\frac{d\Omega}{dr}\right\}+2(\mu+\gamma\epsilon_r^\Omega)\frac{d\Omega}{dr}+\overline{F}_\phi = 0$$

and the turbulent energy equation as

$$-\frac{1}{r}\frac{d}{dr}\left\{r(\mu+\gamma\epsilon_r^q)\frac{dq}{dr}\right\} = \gamma\epsilon_r^\Omega r^2\left(\frac{d\Omega}{dr}\right)^2-\gamma\frac{K_D q^{\frac{3}{2}}}{l}+\frac{1}{r}\frac{d}{dr}\{\gamma\epsilon_r^p r\Omega^2\},$$

where the diffusivity terms are given by relations of the form

$$\epsilon_j^i = K_j^i f^+ l(r)\, q^{\frac{1}{2}}$$

and K_D is Prandtl's dissipation factor.

Here f^+ is a function used to smooth Kjellström's experimental observations: it rises from zero at $y^+ = 0$, passes through 0·5 at $y^+ = 24{\cdot}88$ and tends to 1 for $y^+ \to \infty$. It has been taken as

$$f^+ = 0{\cdot}5 + [\tan^{-1}\{1{\cdot}93 \ln (y^+/24{\cdot}88)\}]/\pi,$$

where $y^+ = y_{\text{wall}}(\tau_{\text{wall}}\gamma/\mu)^{\frac{1}{2}}$ = dimensionless wall distance. The length scale $l(r)$ is given by

$$1/l(r) = 1{\cdot}14 \int_0^{2\pi} d\phi/y.$$

The K values used are those matching fully developed flow in a straight cylindrical tube, namely

$$K_r^{\Omega} = 0{\cdot}427, \quad K_r^q = 0{\cdot}22, \quad K_r^p = 0, \quad K_D = 0{\cdot}176.$$

Values of $\overline{F}_\phi$ and τ_{wall} were obtained from the measured mean of $\overline{F}_\phi$ over the chamber length,

$$\overline{F}_\phi \approx 8{\cdot}3 \times 10^6 \rho B_0^2 (1 + 0{\cdot}81\rho^6)\,\text{N/m}^3.$$

With the boundary conditions $d\Omega/dr$ and dq/dr both zero at $r = 0$, Ω and q both zero at $r = R$, convergent computer solutions for Ω and q were obtained by a finite-difference method.

REFERENCES

Bednarz, T. K. 1970 An experimental investigation of electromagnetic stirring in a coreless induction furnace. Ph.D. thesis, Carnegie–Mellon University, Pittsburgh, Penn.

Bellhouse, B. J. & Schultz, D. L. 1967 The determination of fluctuating velocity in air with heated thin film gauges. *J. Fluid Mech.* **29**, 289–295.

Bradbury, L. J. S. & Castro, I. P. 1971 A pulsed-wire technique for velocity measurements in highly turbulent flows. *J. Fluid Mech.* **49**, 657–691.

Bradshaw, P. 1971 *An Introduction to Turbulence and its Measurement.* Pergamon.

Briskman, V. A., Ermakov, O. I., Rudakov, V. K. & Fedotov, V. M. 1970 Turbulent flow of liquid metal due to a rotating magnetic field. *Gos. Univ., Perm, Uchenye Zapiski*, **216**, 255–261.

Dahlberg, E. 1972 On the action of a rotating magnetic field on a conducting liquid. *AB Atomenergi, Studsvik, Sweden, Rep.* AE-447.

Gerlach, G. 1972 Reaktor für Flüssigmetalle. *Chemie-Ing.-Tech.* **44**, 379.

Greenspan, H. P. 1968 *The Theory of Rotating Fluids*, p. 5. Cambridge University Press.

Hayes, D. J., Baum, M. R. & Hobdell, M. R. 1971 The performance and applications of an electromagnetic rotary-flow device in liquid sodium. *J. Br. Nucl. Energy Soc.* **10**, 93.

Hill, J. C. & Sleicher, C. A. 1971 Directional sensitivity of hot film sensors in liquid metals. *Rev. Sci. Instrum.* **42**, 1461–1468.

Hinze, J. O. 1959 *Turbulence*, pp. 184–185. McGraw-Hill.

Hoff, M. 1969 Hot film anemometry in liquid mercury. *Instrum. & Control Systems*, **42**, 83–86.

Hunt, J. C. R. & Malcolm, D. G. 1968 Some electrically driven flows in magnetohydrodynamics. *J. Fluid Mech.* **33**, 775–801.

Kapusta, A. B. 1969 On the theory of centrifugal casting in a rotating magnetic field. *Magnitnaya Gidrodinamika*, **11**, 117–120.

Kjellström, B. 1972 Transport processes in turbulent channel flow. *Swedish Board for Tech. Development, Stockholm, Rep.* no. 70–409/U 340.

LARSSON, K. 1973 Appendix to "Applications of MHD in metallurgy". *Swedish Board for Tech. Development, Fack, Stockholm, Rep.* no. 72–392/U 312.

LIGHTHILL, M. J. 1954 The response of laminar skin friction and heat transfer to fluctuations in the stream velocity. *Proc. Roy. Soc.* A **224**, 1–23.

MALCOLM, D. G. 1969*a* *DISA Inf.* no. 9.

MALCOLM, D. G. 1969*b* Some aspects of turbulence measurement in liquid mercury using cylindrical quartz-insulated hot-film sensors. *J. Fluid Mech.* **37**, 701–713.

MOFFATT, H. K. 1965 On fluid flow induced by a rotating magnetic field. *J. Fluid Mech.* **22**, 521–528. (Corrigendum 1973 *J. Fluid Mech.* **58**, 823.)

OWER, E. & PANKHURST, R. C. 1966 *The Measurement of Air Flow*, pp. 45–46. Pergamon.

PERRY, A. E. & MORRISON, G. L. 1971 A study of the constant-temperature hot-film anemometer. *J. Fluid Mech.* **47**, 577–599.

PRANDTL, L. 1945 Über ein neues Formelsystem für die ausgebildete Turbulenz. *Nachr. Akad. Wiss. Göttingen, Math.-phys. Klasse*, pp. 6–19. (See also 1961 *Ludwig Prandtl Gesammelte Abhandlungen, Berlin*, pp. 847–887.)

REZIN, N. G., ERMAKOV, O. I. & VETROV, B. G. 1967 A stator for electromagnetic stirring in continuous casting of pig-iron. *Proc. Conf. Applic. Electro-Hydrodyn. in Industry, Trudy* no. 6, *Don. Sci. Res. Inst. for Ferrous Met.* pp. 246–249. Moscow: Izdatelstvo Metallurgia.

SAJBEN, M. 1965 Hot-wire anemometer in liquid mercury. *Rev. Sci. Instrum.* **36**, 945–949.

SCHLICHTING, H. 1968 *Boundary-Layer Theory*, pp. 246–271. McGraw-Hill.

VEDKALOV, I. R., KAPUSTA, A. B., POVKH, I. I., ROTMISTOVSKII, B. M., KOSHELEV, V. A. & TOLSKII, A. A. 1971 Electromagnetic pilot-plant for the treatment of molten metal in a flow. *Magnitnaya Gidrodinamika*, no. 4, 127–132.